Applied Catalysis B: Environmental 314 (2022) 121503

Contents lists available at ScienceDirect

Applied Catalysis B: Environmental

journal homepage: www.elsevier.com/locate/apcatb

Hollow carbon sphere-supported Pt/CoO_x hybrid with excellent hydrogen evolution activity and stability in acidic environment

Yaru Wang [a], Bicheng Zhu [b], Bei Cheng [a], Wojciech Macyk [c], Panyong Kuang [b,*], Jiaguo Yu [a,b,**]

[a] State Key Laboratory of Advanced Technology for Materials Synthesis and Processing, Wuhan University of Technology, Wuhan 430070, PR China
[b] Laboratory of Solar Fuel, Faculty of Materials Science and Chemistry, China University of Geosciences, Wuhan 430074, PR China
[c] Faculty of Chemistry, Jagiellonian University, ul. Gronostajowa 2, 30-387 Kraków, Poland

ARTICLE INFO

Keywords:
Co-based oxides
Acidic hydrogen evolution reaction
Pt/CoO_x-HCS
In situ Raman spectroscopy
Strong electronic interaction

ABSTRACT

Electrocatalytic hydrogen evolution reaction (HER) in acidic solution using Co-based oxides is extremely difficult due to their instability. Herein, we report a hollow carbon sphere-supported Pt/CoO_x (Pt/CoO_x-HCS) electrocatalyst for active HER in 0.5 M H_2SO_4 solution. Microstructural and electrochemical evaluations confirm the dissolution of major Co_3O_4 in Pt/Co_3O_4-loaded HCS (pre-Pt/Co_3O_4-HCS) and the steady existence of remaining CoO_x in Pt/CoO_x-HCS after 3000 cyclic voltammetry (CV) cycles (Pt/CoO_x-HCS-3000). The Pt/CoO_x-HCS-3000 exhibits a pretty high turnover frequency (TOF) of 24.87 H_2 s^{-1} at 100 mV overpotential, a low overpotential of 28 mV at 10 mA cm^{-2}, and a large mass activity of 3.59 A mg_{Pt}^{-1} at 30 mV overpotential. The robust stability of Pt/CoO_x-HCS-3000 is attributed to the strong electronic interaction between Pt and CoO_x, preventing the aggregation of the former and the thorough dissolution of the latter. This work provides insights into the design of Co based-oxide electrocatalysts with outstanding acidic performances.

1. Introduction

Hydrogen (H_2) is a renewable energy carrier with the merit of high energy density, which shows excellent superiority as an alternative to replace traditional fossil fuels [1–5]. Hydrogen evolution reaction (HER) from the electrochemical water splitting is a sustainable and environmentally-friendly strategy to produce H_2, which has received wide attention recently [6–10]. Despite the best HER performance of the precious Pt electrocatalyst, its rare reserves and high costs limit the large-scale applications [11–16]. Therefore, developing earth-abundant, low-cost, and highly active electrocatalysts is an appealing yet challenging task [17–21].

Recently, Co-based oxides have gained extensive research interest and shown great potential as HER electrocatalysts due to their natural abundance and unique 3*d* electronic configuration [22,23]. A great deal of Co-based oxides, including N-Co_3O_4 @C [24], Co/Co_3O_4 [25], P-Co_3O_4 [26] and CoO_x@CN [27], have been fabricated and exhibited outstanding HER performances. Note that almost all the Co-based oxides were used as electrocatalysts in alkaline solution while rare in acidic solution due to their acidic instability feature [28,29]. Unfortunately, the inevitable dissolution would lead to their unstable and inactive behaviors [30]. Despite these issues, it is still reasonably necessary to study the acidic HER performance of electrocatalyst because the HER activity in acidic solution is usually 2–3 orders of magnitude higher than in alkaline solution [31]. Therefore, developing effective strategies to stabilize Co-based oxides in acidic solution is significant for obtaining highly efficient HER activity.

As one of the intrinsic characteristics, the electronic structure plays a significant role in modulating the activity and stability of Co-based oxides [32–35]. Very recently, Huang et al. modified the electronic structure of Co_3O_4 by introducing the nanocrystalline CeO_2 [36]. The created positive local bonding environment in Co_3O_4 allows the easy oxidation of Co^{3+} ions to catalytically active Co^{4+} ions, which avoids the bias-dependent surface reconstruction process in Co_3O_4 and endows the Co_3O_4/CeO_2 hybrid with enhanced acidic OER activity and stability. Despite the enhanced performance for acidic OER, as far as we know, there are rare research works paid attention to improving the activity and stability of Co-based oxides for acidic HER. Recently, noble metals (e.g., Pt and Ru) have significantly enhanced the acidic HER activity and stability of transition metal (hydro)oxides by modulating the electronic

* Corresponding author.
** Corresponding author at: State Key Laboratory of Advanced Technology for Materials Synthesis and Processing, Wuhan University of Technology, Wuhan 430070, PR China.
E-mail addresses: kuangpanyong@cug.edu.cn (P. Kuang), yujiaguo93@cug.edu.cn (J. Yu).

https://doi.org/10.1016/j.apcatb.2022.121503
Received 15 March 2022; Received in revised form 23 April 2022; Accepted 9 May 2022
Available online 11 May 2022

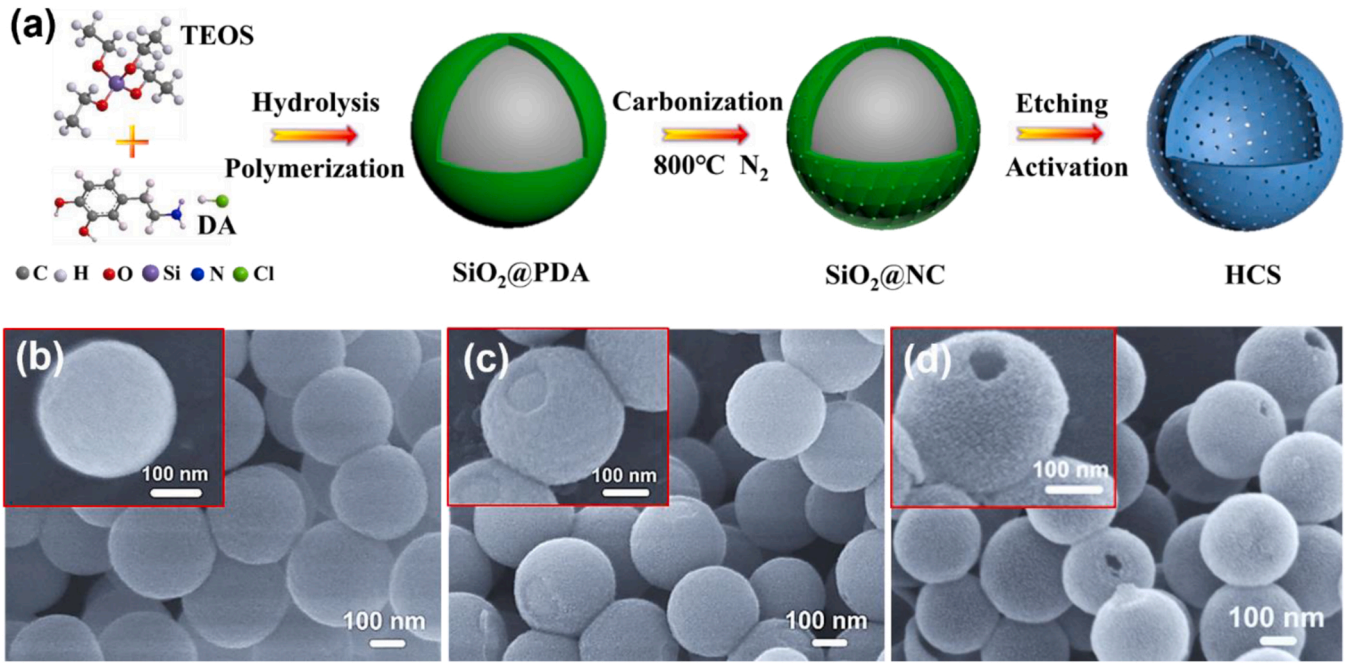

Fig. 1. (a) Schematic illustration for the formation process of the HCS. Step I: Synthesis of the SiO_2 @PDA in the presence of TEOS and DA. Step II: Carbonization of the SiO_2 @PDA to form SiO_2 @NC. Step III: Etching and activation treatments of the SiO_2 @NC to obtain HCS. Scanning electron microscopy (SEM) images of the (b) SiO_2 @PDA, (c) SiO_2 @NC, and (d) HCS.

structures and optimizing the hydrogen adsorption free energies [37, 38]. For example, Xu et al. prepared a single Pt atom-loaded defective MoO_X electrocatalyst, which exhibited an ultrahigh mass activity of 52.0 A mg_{Pt}^{-1} at an overpotential of 50 mV and outstanding long-term stability for 20 h in 0.5 M H_2SO_4 solution. The experimental and theoretical studies reveal that the strong electronic interaction in this hybrid tunes the electronic structure of Pt atom and optimizes the adsorption behavior for hydrogen atoms [37]. Wang et al. synthesized a ternary electrocatalyst comprising polyaniline, Ru cluster, and $Ni(OH)_2$ nanosheet. Attributed to the synergistic effect among these components, such a ternary polyaniline-coated $Ru/Ni(OH)_2$ electrocatalyst displayed a comparable HER activity to 20 wt% Pt/C in 0.5 M H_2SO_4 solution [38].

Inspired by these achievements, herein, we fabricated a HCS-supported Pt/CoO_x (Pt/CoO_x-HCS) electrocatalyst, which exhibits highly active HER activity and stability in acidic solution. The Pt/CoO_x-HCS was in situ prepared by performing successive CV cycles to the pre-Pt/Co_3O_4-HCS. The major Co_3O_4 in pre-Pt/Co_3O_4-HCS is dissolved after operating 3000 CV cycles, and the remaining CoO_x in Pt/CoO_x-HCS-3000 could steadily exist via the strong electronic interaction with Pt. At a low Pt loading content of 1.05 wt%, the Pt/CoO_x-HCS-3000 exhibits an excellent acidic HER activity in 0.5 M H_2SO_4 solution, i.e. a pretty high TOF of 24.87 H_2 s^{-1} at an overpotential of 100 mV, a low η_{10} value of 28 mV, and a large mass activity of 3.59 A mg_{Pt}^{-1} at an overpotential of 30 mV (ca. 30-fold larger than 20 wt% Pt/C). Further spectroscopic characterizations and theoretical studies reveal that the strong electronic interaction could prevent the aggregation and dissolution of the Pt and CoO_x, respectively, which should be responsible for the extraordinary stability in acidic solution. We hope this work could provide insights into the design of Co-based oxide electrocatalysts with outstanding acidic activity and stability for diverse fields.

2. Experimental section

2.1. Materials and chemicals

Tetraethyl orthosilicate ($C_8H_{20}O_4Si$, TEOS), dopamine hydrochloride (DA), ammonia ($NH_3{\cdot}H_2O$, 28 wt%), hydrofluoric acid (HF, 10 wt %), potassium hydroxide (KOH), hydrochloric acid (HCl), ethanol (C_2H_6O), ethylene glycol ($C_2H_6O_2$), sodium borohydride ($NaBH_4$), chloroplatinic acid hexahydrate ($H_2PtCl_6{\cdot}6\ H_2O$) and cobalt acetate tetrahydrate ($Co(CH_3COO)_2{\cdot}4\ H_2O$) were purchased from Sinopharm Chemical Reagent Co., Ltd. Commercial 20 wt% Pt/C was purchased from Johnson Matthey Company and 5 wt% Nafion ethanol solution was afforded by DuPont Company.

2.2. Preparation of the HCS

Hollow carbon sphere (HCS) was prepared according to our previously reported work. Firstly, 1 mL of TEOS, 1 mL of $NH_3{\cdot}H_2O$ (28 wt%) and 24 mL of ethanol were added into 80 mL of distilled water, which was stirred for 30 min. Then, 8 mL of the DA solution was added into the above-mixed solution and stirred for 24 h at room temperature. After the completion of reaction, the polydopamine-coated SiO_2 (SiO_2 @PDA) sphere were obtained by centrifugation, then washed with distilled water/ethanol and dried at 80 °C for 24 h. Subsequently, the SiO_2 @PDA sphere were calcined at 800 °C for 2 h under N_2 atmosphere to form the N-doped carbon-covered SiO_2 (SiO_2 @NC) sphere. Finally, the HCS was obtained through the etching method followed by alkaline activation treatment. In detail, SiO_2 @NC was dispersed into HF solution and kept stirring for 1 h to remove the core of SiO_2. After finishing the wash, collection and desiccation processes, the resultant products were then mixed with KOH and annealed at 800 °C for 3 h under N_2 atmosphere to form HCS. After that, the HCS with residual KOH was washed with HCl aqueous solution (10 wt%) and distilled water several times and dried at 80 °C for 24 h.

2.3. Preparation of the pre-Pt/Co_3O_4-HCS, pre-Pt-HCS, and pre-Co_3O_4-HCS

Firstly, 50 mg of HCS was added into 50 mL of ethylene glycol and kept stirring for 1 h. Secondly, 15.45 mg of $Co(CH_3COO)_2{\cdot}4\ H_2O$ and 1.785 mL of $H_2PtCl_6{\cdot}6\ H_2O$ solution (2 mg mL^{-1}) were added into the above suspension and kept mild stirring for another 3 h. Afterward, the mixed solution was placed into an oil bath and heated up to 120 °C, and

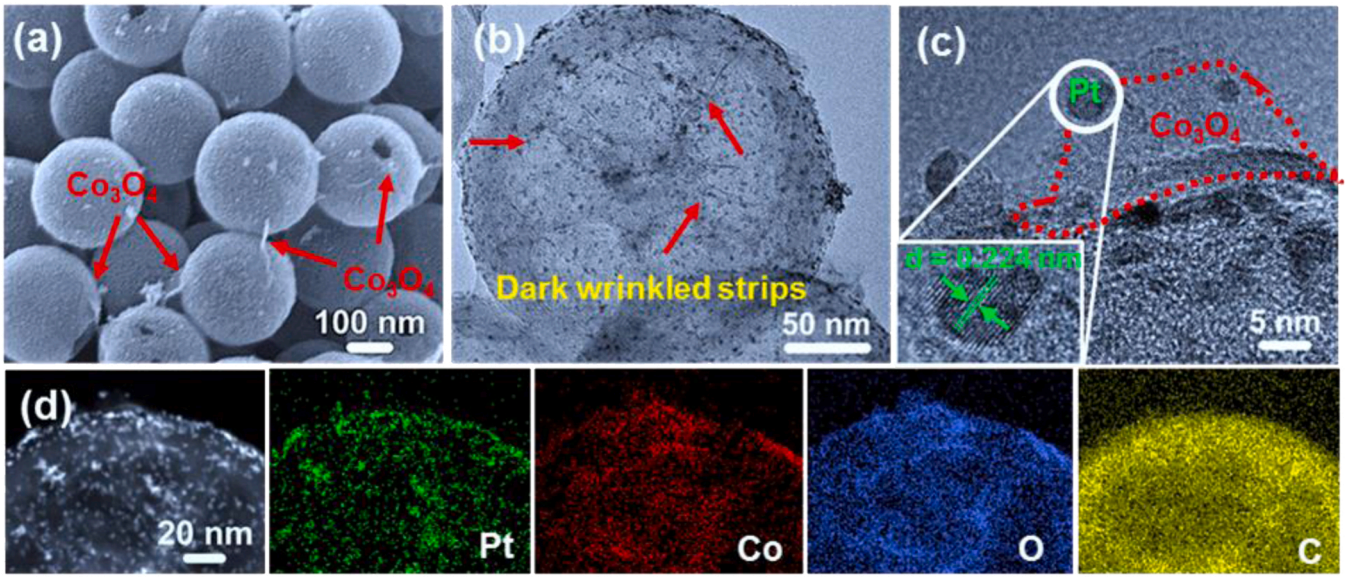

Fig. 2. (a) SEM, (b) TEM, (c) HRTEM, and (d) EDX elemental mapping images of the pre-Pt/Co_3O_4-HCS.

10 mL of the $NaBH_4$ solution (10 mg mL^{-1}) was then slowly added into the solution under vigorous stirring. After fully reacting at 120 °C for 0.5 h, the pre-Pt/Co_3O_4-HCS electrocatalyst was obtained by centrifugation, then washed with distilled water several times and dried at 80 °C for 24 h. According to the inductively coupled plasma-optical emission spectrometry (ICP-OES) measurement, the actual loading contents of Pt and Co are measured to be 1.05 wt% and 3.29 wt%, respectively. For comparison, the pre-Pt-HCS electrocatalyst with Pt loading content of 1.05 wt% (denoted as pre-Pt-HCS (1.05)) was prepared through the same synthetic process by adding 1.785 mL of $H_2PtCl_6.6\ H_2O$ solution (2 mg mL^{-1}) alone.

The synthetic processes of pre-Pt-HCS and pre-Co_3O_4-HCS were similar to those of the pre-Pt/Co_3O_4-HCS without adding Co $(CH_3COO)_2{\cdot}4\ H_2O$ and $H_2PtCl_6{\cdot}6\ H_2O$ solution, respectively. Specifically, the pre-Pt-HCS was prepared by adding 6.635 mL of $H_2PtCl_6{\cdot}6\ H_2O$ solution (2 mg mL^{-1}) alone, and the actual loading content of Pt was examined to be 8.22 wt%. The pre-Co_3O_4-HCS was prepared by using 21.13 mg of $Co(CH_3COO)_2{\cdot}4\ H_2O$ alone, and the actual loading content of Co was examined to be 7.08 wt%.

2.4. Preparation of the Pt/CoO_x-HCS-3000, Pt-HCS-3000, and Co_3O_4-HCS-3000

The Pt/CoO_x-HCS-3000 was prepared through successive CV cycles on pre-Pt/Co_3O_4-HCS. To tested the stability of pre-Pt/Co_3O_4-HCS, which after performing 3000, 10,000, 15000, and 20,000 CV cycles was denoted as Pt/CoO_x-HCS-3000, Pt/CoO_x-HCS-10,000, Pt/CoO_x-HCS-15,000, and Pt/CoO_x-HCS-20,000, respectively. CV measurement was conducted in a potential region of 0 to − 0.1 V (vs. RHE) with a scan rate of 100 mV s^{-1}. Such a definition was also employed to other counterparts after different CV cycles.

3. Results and discussion

3.1. Morphological and microstructural characterizations

Fig. 1a presents the synthetic process of the HCS. In brief, HCS with an average diameter of ~300 nm was prepared by performing the hydrolysis/polymerization, carbonization, etching, and alkaline activation strategies (Fig. 1b-d) (See experimental details Supplementary Information) [39–42]. The alkaline activation endows HCS with high porosity and ultrahigh specific surface area of up to 2556 $m^2\ g^{-1}$ (Fig. S1), which is conducive to the homogeneous distribution of active sites and the creation of efficient three-phase reaction regions for electron transfer, ion transport, and gas diffusion [6,43,44]. Using HCS as a support, HCS-supported Pt/Co_3O_4, Pt, and Co_3O_4 (pre-Pt/Co_3O_4-HCS, pre-Pt-HCS, and pre-Co_3O_4-HCS, respectively) were fabricated and used as the pre-catalyst for acidic HER study.

Fig. 2a shows the SEM image of the pre-Pt/Co_3O_4-HCS (Pt: 1.05 wt%, Co: 3.29 wt%). Co_3O_4 nanosheets (NSs) are randomly wrapped on the surface of HCS, which is further confirmed by the dark wrinkled strips in the transmission electron microscopy (TEM) image (Fig. 2b). Moreover, Pt nanoparticles (NPs) with an diameter of 2–4 nm are uniformly distributed on the HCS without apparent aggregation (Figs. 2b and S2), which is considered to benefit from the ultrahigh specific surface area of the HCS [45]. High-resolution TEM (HRTEM) image (Fig. 2c) shows the intimate contact of Pt NPs and Co_3O_4 NSs, which creates opportunities for Pt to alter the electronic structure of CoO_x and thereby induces strong electronic interaction. The Pt marked with a white circle displays the (111) facet with a lattice finger of 0.224 nm [46], and the Co_3O_4 in the red dashed region presents a low crystallization feature. Note that characteristic peaks of the Pt and Co_3O_4 are undetectable in the X-ray diffraction (XRD) pattern due to their low content (Fig. S3). In contrast, such peaks are detected for the pre-Pt-HCS and pre-Co_3O_4-HCS with high loading content of Pt (8.22 wt%) and Co (7.08 wt%), respectively (Figs. S4 and S5). Fig. 2d displays the energy-dispersive X-ray (EDX) elemental mapping images, and the elements of Pt, Co, and O are homogeneously distributed on HCS. More importantly, the elemental mapping images of Co and O show strong signals correspond to the red dashed region in Fig. 2c, which strongly verifies the existence of Co_3O_4. Based on the above discussion, it can be concluded that the pre--Pt/Co_3O_4-HCS electrocatalyst was successfully prepared.

3.2. CV cycles treatment

Because the HER activity was evaluated in an acidic solution (0.5 M H_2SO_4) and Co_3O_4 would suffer from the acidic dissolution, it is necessary to conduct the pretreatment for pre-Pt/Co_3O_4-HCS to reach a steady state. Therefore, we performed uninterrupted CV cycles to the pre-Pt/Co_3O_4-HCS in 0.5 M H_2SO_4 solution. The adopted potential region for CV cycle (0 ~ −0.1 V vs. RHE) could reduce Co^{3+} ions to Co^{2+} ions but can't further reduce Co^{2+} ions to metallic Co. Furthermore, according to the theoretical and experimental Pourbaix diagram of Co-based oxides, the two factors of pH value and reductive potential

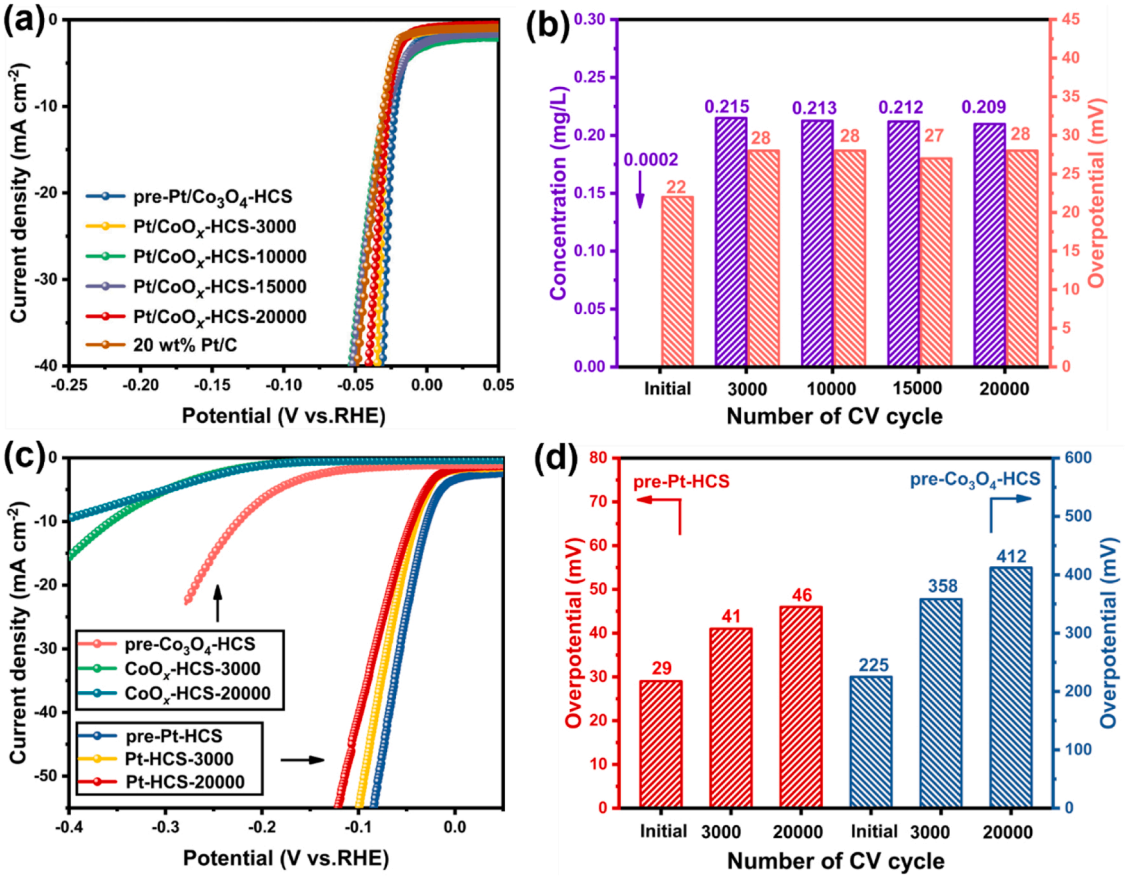

Fig. 3. (a) LSV curves of the 20 wt% Pt/C and pre-Pt/Co_3O_4-HCS at different CV cycle, and (b) the corresponding changes in η_{10} value and concentration of Co element. (c) LSV curves of the pre-Pt-HCS and pre-Co_3O_4-HCS at different CV cycle, and (d) the corresponding changes in η_{10} value.

region in this work together determine that the reduced product would not present in Co metallic state [47]. As presented in Fig. 3a, the pre--Pt/Co_3O_4-HCS exhibits an initial η_{10} value of 22 mV to deliver a current density of 10 mA cm^{-2}, and this value for Pt/CoO_x-HCS-3000 slightly increases to 28 mV. Surprisingly, with proceeding the CV cycle, the η_{10} value remains almost the same for Pt/CoO_x-HCS-10,000 (η_{10} = 28 mV), Pt/CoO_x-HCS-15,000 (η_{10} = 27 mV), and Pt/CoO_x-HCS-20,000 (η_{10} = 28 mV), respectively, suggesting that the dissolution of major Co_3O_4 has already completed after 3000 CV cycles. More importantly, the Pt/CoO_x-HCS-3000 still exhibits a comparable η_{10} value to the 20 wt% Pt/C benchmark electrocatalyst (η_{10} = 30 mV). In addition to the η_{10} value, the changes in Co element concentration in electrolyte also prove the steady state of Pt/CoO_x-HCS-3000. As displayed in Fig. 3b, the concentration of Co element determined by ICP-OES measurement dramatically increases from near 0 mg L^{-1} in the initial electrolyte to 0.215 mg L^{-1} in the electrolyte after 3000 CV cycles, then remains almost parallel with further proceeding the CV cycle to 10,000 (0.213 mg L^{-1}), 15,000 (0.212 mg L^{-1}), and 20,000 (0.209 mg L^{-1}). Analogously, there is a remarkable increase in Co element concentration (from near 0–0.451 mg L^{-1}) in electrolyte after 3000 CV cycles for pre-Pt/Co_3O_4-HCS and the concentrations are maintained at high levels with further proceeding CV cycles (Fig. S6), suggesting the almost thorough dissolution of Co_3O_4 in the absence of Pt NPs, which is also evidenced by the following spectroscopic investigations. Therefore, the results of CV cycles and ICP-OES measurements strongly confirm the steady state of Pt/CoO_x-HCS-3000.

In addition, CV cycles were conducted to the counterpart of pre-Pt-HCS with a Pt loading content of 1.05 wt% (denoted as pre-Pt-HCS (1.05)). As presented in Fig. S7, the pre-Pt-HCS (1.05) exhibits an initial η_{10} value of 42 mV, larger than that of the pre-Pt/Co_3O_4-HCS (22 mV), suggesting that the incorporation of Pt and Co_3O_4 greatly contributes to the improved HER activity. Dramatically, the η_{10} value of Pt-HCS (1.05)-3000 significantly increases to 74 mV, much larger than that of the Pt/CoO_x-HCS-3000 (28 mV), which may be attributed to the aggregation or dissolution of Pt NPs in the absence of CoO_x. We thus conclude that the Co_3O_4 is not thoroughly dissolved and the remaining CoO_x plays a significant role in enhancing the stability of Pt NPs. Besides, CV cycles on another two counterparts of pre-Pt-HCS and pre-Co_3O_4-HCS were conducted as well. As shown in Fig. 3c and d, the η_{10} value of the pre-Pt-HCS and pre-Co_3O_4-HCS increases linearly with increasing the number of CV cycles, revealing the poor stability of the individual Pt and CoO_x alone. TEM images present the severe aggregation of Pt NPs in Pt-HCS-3000 after 3000 CV cycles (Fig. S8). Moreover, CoO_x was almost completely dissolved in CoO_x-HCS-3000 after 3000 CV cycles, as evidenced by the TEM images and XPS spectra (Figs. S9 and S10). The above results strongly indicate that there must be strong interactions between Pt and CoO_x, which prevents the aggregation of the former and the thorough dissolution of the latter.

3.3. Hydrogen evolution reaction performance

We then comprehensively evaluated the HER performance of the Pt/CoO_x-HCS-3000, which has reached a steady state in 0.5 M H_2SO_4 solution. As shown in Fig. 4a-c and Table S2, the Pt/CoO_x-HCS-3000 offers a η_{10} value of 28 mV, which is considerably smaller than that of the 20 wt% Pt/C (30 mV) and Pt-HCS-3000 (41 mV), and even exceeds other HER electrocatalysts reported recently, such as Pd_1-$CoSe_2$ (80 mV) [48], PtN_x/TiO_2 (67 mV) [49] and Ru-NiCoP/NF (44 mV) [50]. Furthermore, Pt/CoO_x-HCS-3000 possesses a large mass activity of 3.59 A mg_{Pt}^{-1} at an overpotential of 30 mV (Figs. 4b and S11), which is

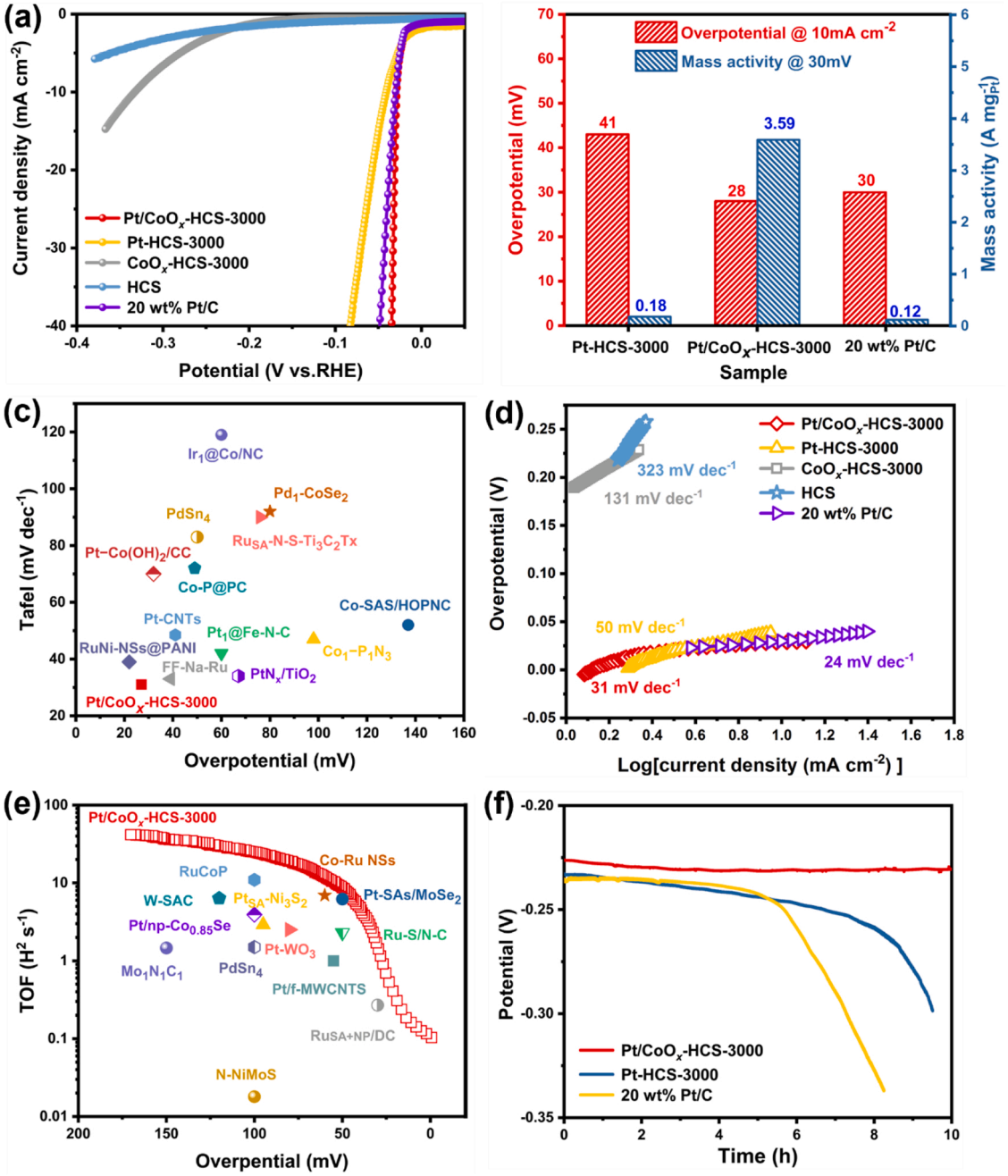

Fig. 4. (a) LSV curves of the Pt/CoO_x-HCS-3000, Pt-HCS-3000, CoO_x-HCS-3000, HCS, and 20 wt% Pt/C, and (b) the corresponding mass activity and η_{10} values. (c) The comparison of η_{10} value and Tafel slope between the Pt/CoO_x-HCS-3000 and other recently reported HER electrocatalysts. (d) Tafel slope of the Pt/CoO_x-HCS-3000, Pt-HCS-3000, CoO_x-HCS-3000, HCS, and 20 wt% Pt/C. (e) TOF values of the Pt/CoO_x-HCS-3000 and other recently reported HER electrocatalysts. (f) Chronopotentiometry tests of the Pt/CoO_x-HCS-3000, Pt-HCS-3000, and 20 wt% Pt/C.

about 20 and 30-fold larger than that of the Pt-HCS-3000 and 20 wt% Pt/C at the same overpotential, suggesting the significantly enhanced Pt utilization in Pt/CoO_x-HCS-3000. In addition, Pt/CoO_x-HCS-3000 exhibits a quite low Tafel slope of 31 mV dec^{-1}, indicating a similar reaction pathway to the 20 wt% Pt/C with significantly promoted reaction kinetics (Fig. 4c and d). Besides, the TOF values of Pt/CoO_x-HCS-3000 are higher than most reported HER electrocatalysts in the overpotential region from 50 to 200 mV. For example, Pt/CoO_x-HCS-3000 possesses a TOF value of 24.87 H_2 s^{-1} at an overpotential of 100 mV, which is much higher than that of the RuCoP (10.95 H_2 s^{-1}) [51], Pt/np-$Co_{0.85}Se$ (3.93 H_2 s^{-1}) [52], Pt-PMo/ZIF-67–800 (1.3 H_2 s^{-1}) [53] and 20 wt% Pt/C (2.12 H_2 s^{-1} in this work) (Fig. 4e and Table S3), revealing the superb HER activity. Additionally, chronopotentiometry tests under 10 mA cm^{-2} prove the highly-robust stability of the Pt/CoO_x-HCS-3000. As shown in Fig. 4f, the Pt/CoO_x-HCS-3000 shows a negligible increment in the applied potential (~3 mV) after 10 h successive operation, whereas the increment sharply rises to 101 and 139 mV for the Pt-HCS-3000 and 20 wt% Pt/C, respectively. The superior intrinsic activity of Pt/CoO_x-HCS-3000 can be further verified by electrochemically active surface area (ECSA) and electrochemical impedance spectroscopy (EIS) measurements. As shown in Fig. S12, Pt/CoO_x-HCS-3000 exhibits a double-layer capacitance (C_{dl}) value of 56.4 mF cm^{-2}, which is greater than that of the Pt-HCS-3000 (47.8 mF cm^{-2}) and CoO_x-HCS-3000 (25.5 mF cm^{-2}), suggesting the increased number of active sites. Moreover, Pt/CoO_x-HCS-3000 shows a much lower charge transfer resistance (R_{ct}, 2.58 Ω) than that of the Pt-HCS-3000 (20.05 Ω) and CoO_x-HCS-3000

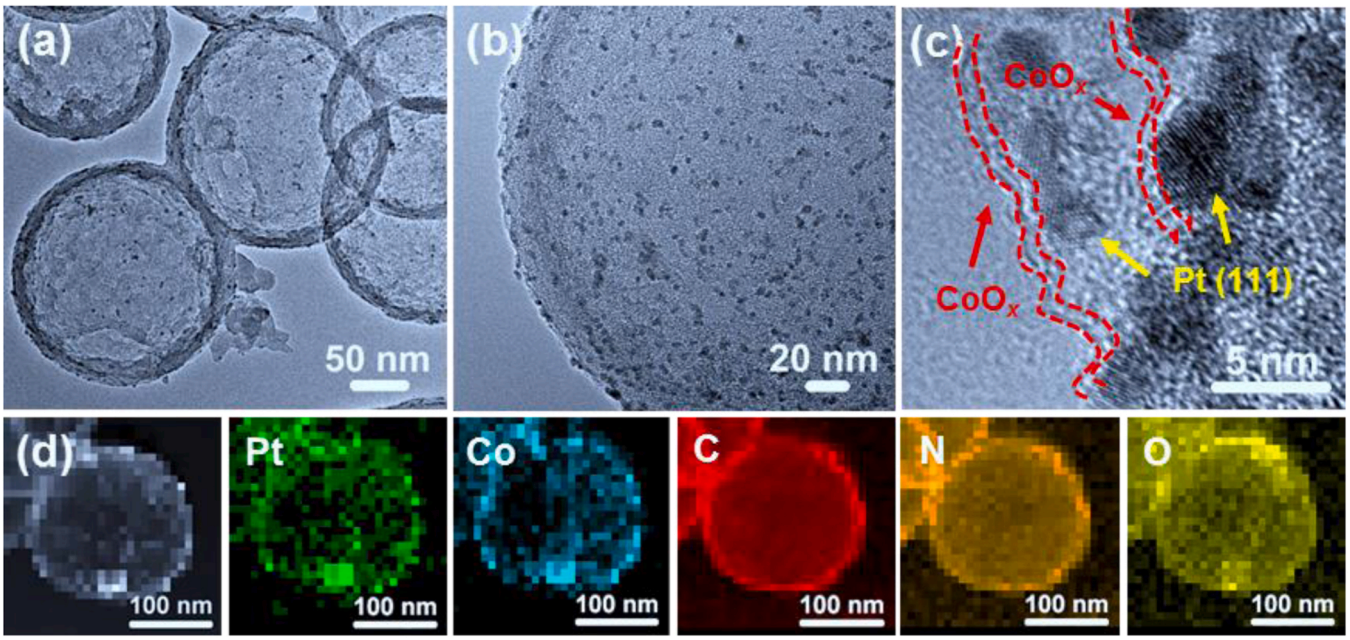

Fig. 5. (a, b) TEM, (c) HRTEM, and (d) EDX elemental mapping images of the Pt/CoO_x-HCS-3000.

(66.77 Ω), revealing the promoted electron transfer ability in Pt/CoO_x hybrid with strong electronic interaction (Fig. S13).

3.4. The analysis of in situ Raman spectroscopy and XPS spectra

The preceding results reveal the superb acidic HER activity and stability of the Pt/CoO_x-HCS-3000. Fig. 5a and b display the TEM images of the Pt/CoO_x-HCS-3000, which can be seen that Pt NPs are still homogeneously distributed on the HCS without apparent aggregation. HRTEM image shows that few CoO_x closely contact with the Pt NPs (Fig. 5c). Moreover, EDX elemental mapping images reveal the uniform distribution of Co and O elements over the HCS (Fig. 5d).

To further confirm the remaining CoO_x and unveil its electronic interaction with Pt, the in situ Raman spectroscopy measurements were conducted in 0.5 M H_2SO_4 solution under HER conditions. As indicated in Fig. 6a and b, the initial spectra of both the pre-Pt/Co_3O_4-HCS and pre-Co_3O_4-HCS show three characteristic Raman peaks, corresponding to the E_g (~472 cm^{-1}), $F_{2\,g}$ (~520 cm^{-1}), and $A_{1\,g}$ (~672 cm^{-1}) modes of Co_3O_4 [54,55]. Raman intensities of the E_g and $F_{2\,g}$ peaks in both the pre-Pt/Co_3O_4-HCS and pre-Co_3O_4-HCS significantly weaken and then disappear after 3000 CV cycles, suggesting the dissolution of Co_3O_4. Interestingly, Raman intensity of the $A_{1\,g}$ peak in the pre-Co_3O_4-HCS significantly decreases and finally disappears after 15,000 CV cycles, indicating that the Co_3O_4 alone is not tolerant to H_2SO_4 solution. Contrarily, although the Raman intensity of the $A_{1\,g}$ peak in the pre--Pt/Co_3O_4-HCS decreases after 3000 CV cycles, it remains almost unchanged with prolonging the CV cycles, which strongly suggests that Pt would greatly promote the stability of CoO_x in acidic solution. In addition to the intensity changes, the pre-Pt/Co_3O_4-HCS shows a continuous blue-shift in the $A_{1\,g}$ peak position with prolonging the CV cycles (Figs. 6a and S14), and the blue-shift in Raman signal is usually derived from the electronic interaction and charge redistribution.

XPS measurements further prove the electronic interaction and charge redistribution between Pt and CoO_x. As shown in Fig. 6c and d, the binding energies of Pt 4 f for the Pt/CoO_x-HCS-3000 negatively shifts to lower values compared to that of the pre-Pt/Co_3O_4-HCS; however, positive shifts of Co 2p binding energies occurred for the Pt/CoO_x-HCS-3000 in comparison with that of the pre-Pt/Co_3O_4-HCS, revealing the electron transfer from CoO_x to Pt. Note that the ratio of Co^{3+} to Co^{2+} in XPS spectra decreases from 2.15 in pre-Pt/Co_3O_4-HCS to 0.54 in Pt/CoO_x-HCS-3000 (Fig. S15), suggesting the successive reduction of Co^{3+} ions. However, Co element is almost undetectable in the XPS spectrum of the CoO_x-HCS-3000 (Fig. S10), which reveals the vital role of Pt in stabilizing the CoO_x in acidic solution. Besides, the electron transfer was further confirmed by work function (WF) [56]. As shown in Fig. 7a and b, WFs values of the Pt-HCS-3000, Pt/CoO_x-HCS-3000, and CoO_x-HCS-3000 were calculated to be 4.63, 4.56, and 4.49 eV, respectively. The lowest WF value of Pt/CoO_x-HCS-3000 strongly confirms the electron transfer from CoO_x to Pt, which is subsequently consumed by the HER process. Therefore, together with the in situ Raman spectroscopy and XPS results, the WF results unveil the strong electronic interaction between Pt and CoO_x, which could stabilize the CoO_x in acidic solution and eventually result in excellent HER activity and stability (Fig. S16).

3.5. DFT calculations

DFT calculations were performed to further certify the electronic interaction between Pt and CoO_x. Given the facts that Co^{2+} species is the main component in CoO_x (Fig. S15), the CoO model is therefore selected to represent the CoO_x in Pt/CoO_x hybrid [57]. The Pt/CoO_x, Pt, and CoO_x possess a Gibbs free energy of H adsorption (ΔG_{H^*}) value of − 0.25, − 0.64, and − 3.16 eV, respectively (Fig. 7c), which suggests that the Pt/CoO_x hybrid is superior to Pt and CoO_x alone in terms of the HER activity [58]. In addition, charge density difference ($\Delta\rho$) shows the electron perturbations in Pt/CoO_x before and after H adsorption. As illustrated in Figs. 7d and S21a-b, electrons are hugely accumulated on the side of Pt along the Pt/CoO_x interface before H adsorption, which is in good agreement with the results of XPS and WF that electrons are transferred from CoO_x to Pt. Furthermore, more electron migrations after H adsorption are confirmed by the Bader charge analysis. Specifically, the electron transfer from CoO_x to Pt is 0.52 eV after H adsorption, which is more than that before H adsorption (0.43 eV), indicating that more free electrons are injected into the active Pt site after H adsorption and then participate in the proton reduction reaction (Figs. 7e and S21c-d). The electron transfer process can promote the Heyrovsky step ($H^+ + e^- + H_{ads} \rightarrow H_2$) and accelerate the release of H_2. Moreover, the density of states (DOS) are shown in the Fig. S22 to reveal the free electronic states near the Fermi level. Compared with pure Pt, the Pt 5d orbital in Pt/CoO_x exhibits higher density near the Fermi level

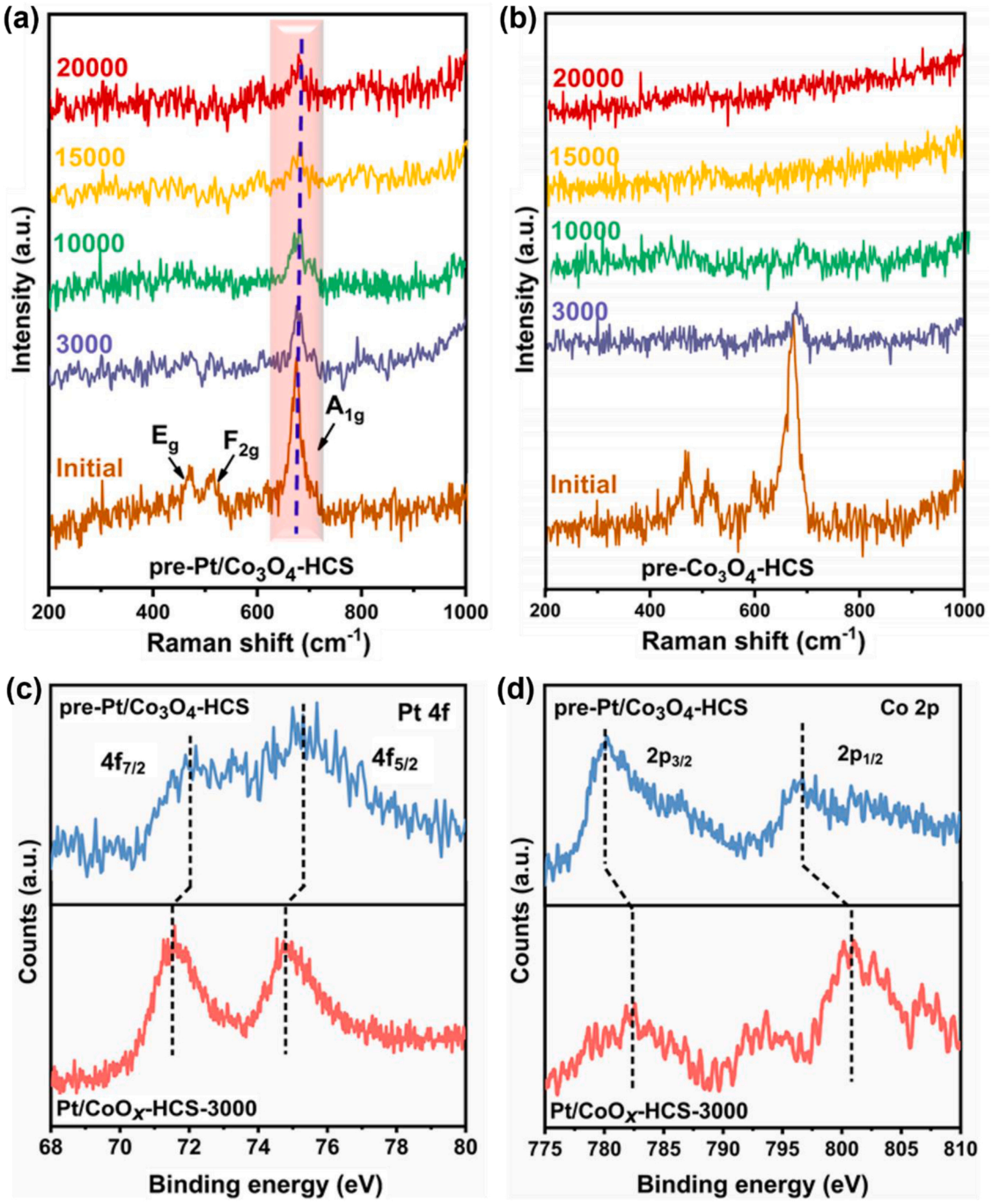

Fig. 6. (a-b) *In-situ* Raman spectroscopies of the pre-Pt/Co_3O_4-HCS and pre-Co_3O_4-HCS at different CV cycle. (c-d) XPS spectra of the Pt 4f and Co 2p for pre-Pt/Co_3O_4-HCS and Pt/CoO_x-HCS-3000, respectively.

due to the introduction of more electrons, which is in accordance with the result of $\Delta\rho$ (Fig. 7d). Contrarily, Pt/CoO_x shows lower occupation in Co 3d orbital relative to Fermi level than that of the CoO_x, suggesting the improved electron transfer property of CoO_x after coupling with Pt, which leads to the electron transfer form Co to Pt [59,60]. Based on the results of spectroscopic and theoretical studies, it is concluded that there are strong electronic interactions between Pt and CoO_x, which greatly contribute to the active HER activity and robust stability of the Pt/CoO_x hybrid in acidic solution.

4. Conclusions

In summary, we have designed and fabricated the Pt/CoO_x-HCS-3000 electrocatalyst through a successive CV cycle strategy. The Pt/CoO_x-HCS-3000 displays highly active and stable HER performances in 0.5 M H_2SO_4 solution. CV cycle experiments reveal the dissolution of major Co_3O_4 in pre-Pt/Co_3O_4-HCS and the steadily remained CoO_x in Pt/CoO_x-HCS-3000 after 3000 CV cycles. Together with the results of CV cycle experiments, the in situ Raman spectroscopy, XPS spectra, WF measurement, and DFT calculations unambiguously reveal the strong electronic interaction between Pt and CoO_x, which prevents the aggregation of the Pt and the thorough dissolution of the CoO_x, and should account for the extraordinary stability in acidic solution. As a result, the Pt/CoO_x-HCS-3000 exhibits an excellent acidic HER activity in 0.5 M H_2SO_4 solution, i.e. a pretty high TOF value of 24.87 H_2 s^{-1} at an overpotential of 100 mV, a low η_{10} value of 28 mV, and a large mass

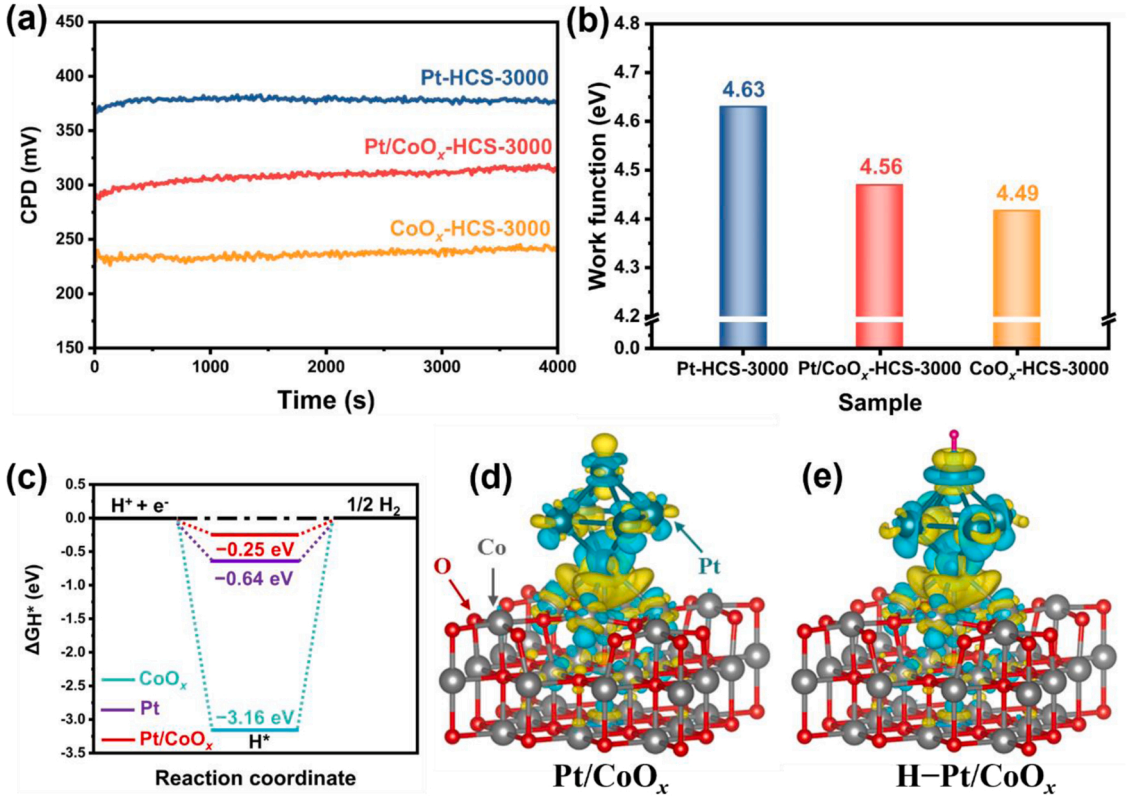

Fig. 7. (a) Contact potential difference (CPD) and (b) corresponding WF value of the Pt-HCS-3000, Pt/CoO_x-HCS-3000, and CoO_x-HCS-3000. (c) ΔG_{H^*} value of the Pt/ CoO_x, Pt, and CoO_x. (d-e) $\Delta\rho$ of the Pt/CoO_x before and after H adsorption. The yellow and cerulean represent the electron accumulation and depletion, respectively.

activity of 3.59 A mg_{Pt}^{-1} at an overpotential of 30 mV (ca. 30-fold larger than 20 wt% Pt/C). This work may offer a new methodology for designing Co-based oxide electrocatalysts with extraordinary acidic activity and stability toward diverse fields.

CRediT authorship contribution statement

Yaru Wang: Methodology, Data curation, Formal analysis, Writing – original draft. **Bicheng Zhu:** DFT Calculations, Data curation. **Bei Cheng:** Data curation, Funding acquisition, Software. **Wojciech Macyk**: Data curation, Software. **Panyong Kuang:** Formal analysis, Conceptualization, Writing – review & editing. **Jiaguo Yu:** Supervision, Conceptualization, Writing – review & editing.

Declaration of Competing Interest

The authors declare that they have no known competing financial interests or personal relationships that could have appeared to influence the work reported in this paper.

Acknowledgments

This work was supported by the National Natural Science Foundation of China (51932007, 51961135303, 22005232, 21871217, U1905215, 52073223, and 21905219).

Appendix A. Supplementary material

Supplementary data associated with this article can be found in the online version at doi:10.1016/j.apcatb.2022.121503.

References

[1] H. Zou, B. He, P. Kuang, J. Yu, K. Fan, Ni_xS_y nanowalls/nitrogen-doped graphene foam is an efficient trifunctional catalyst for unassisted artificial photosynthesis, Adv. Funct. Mater. 28 (2018), 1706917.
[2] F. Luo, H. Hu, X. Zhao, Z. Yang, Q. Zhang, J. Xu, T. Kaneko, Y. Yoshida, C. Zhu, W. Cai, Robust and stable acidic overall water splitting on Ir single atoms, Nano Lett. 20 (2020) 2120–2128.
[3] P. Kuang, T. Tong, K. Fan, J. Yu, In situ fabrication of Ni–Mo bimetal sulfide hybrid as an efficient electrocatalyst for hydrogen evolution over a wide pH range, ACS Catal. 7 (2017) 6179–6187.
[4] Y. Xia, M. Sayed, L. Zhang, B. Cheng, J. Yu, Single-atom heterogeneous photocatalysts, Chem. Catal. 1 (2021) 1173–1214.
[5] Y. Liu, X. Liang, H. Chen, R. Gao, L. Shi, L. Yang, X. Zou, Iridium-containing water-oxidation catalysts in acidic electrolyte, Chin. J. Catal. 42 (2021) 1054–1077.
[6] H. Chen, X. Liang, Y. Liu, X. Ai, T. Asefa, X. Zou, Active site engineering in porous electrocatalysts, Adv. Mater. 32 (2020), 2002435.
[7] P. Kuang, M. He, H. Zou, J. Yu, K. Fan, 0D/3D MoS_2-NiS_2/N-doped graphene foam composite for efficient overall water splitting, Appl. Catal. B Environ. 254 (2019) 15–25.
[8] W. Zang, T. Sun, T. Yang, S. Xi, M. Waqar, Z. Kou, Z. Lyu, Y.P. Feng, J. Wang, S. J. Pennycook, Efficient hydrogen evolution of oxidized Ni-N_3 defective sites for alkaline freshwater and seawater electrolysis, Adv. Mater. 33 (2021), 2003846.
[9] L. Wen, J. Yu, C. Xing, D. Liu, X. Lyu, W. Cai, X. Li, Flexible vanadium-doped Ni_2P nanosheet arrays grown on carbon cloth for an efficient hydrogen evolution reaction, Nanoscale 11 (2019) 4198–4203.
[10] P. Kuang, M. He, B. Zhu, J. Yu, K. Fan, M. Jaroniec, 0D/2D NiS_2/V-MXene composite for electrocatalytic H_2 evolution, J. Catal. 375 (2019) 8–20.
[11] X. Han, X. Wu, Y. Deng, J. Liu, J. Lu, C. Zhong, W. Hu, Ultrafine Pt nanoparticle-decorated pyrite-type CoS_2 nanosheet arrays coated on carbon cloth as a bifunctional electrode for overall water splitting, Adv. Energy Mater. 8 (2018), 1800935.
[12] Z. Liu, J. Li, S. Xue, S. Zhou, K. Qu, Y. Li, W. Cai, Pt/Mo_2C heteronanosheets for superior hydrogen evolution reaction, J. Energy Chem. 47 (2020) 317–323.
[13] J.G. Li, K. Xie, H. Sun, Z. Li, X. Ao, Z. Chen, K.K. Ostrikov, C. Wang, W. Zhang, Template-directed bifunctional dodecahedral CoP/CN@MoS_2 electrocatalyst for high efficient water splitting, ACS Appl. Mater. Interfaces 11 (2019) 36649–36657.
[14] Y. Wang, X. Huang, Z. Wei, Recent developments in the use of single-atom catalysts for water splitting, Chin. J. Catal. 42 (2021) 1269–1286.
[15] J. Yu, A general route via carbon quantum dots assembled to prepare ruthenium based bimetals electrocatalysts for pH-universal hydrogen evolution reaction, Acta Phys. Chim. Sin. 37 (2021), 2011004.

[16] J. Chen, M. Qin, S. Ma, R. Fan, X. Zheng, S. Mao, C. Chen, Y. Wang, Rational construction of Pt/$PtTe_x$ interface with optimal intermediate adsorption energy for efficient hydrogen evolution reaction, Appl. Catal. B Environ. 299 (2021), 120640.

[17] P. Kuang, M. Sayed, J. Fan, B. Cheng, J. Yu, 3D graphene-based H_2-production photocatalyst and electrocatalyst, Adv. Energy Mater. 10 (2020), 1903802.

[18] B. Zhong, P. Kuang, L. Wang, J. Yu, Hierarchical porous nickel supported $NiFeO_xH_y$ nanosheets for efficient and robust oxygen evolution electrocatalyst under industrial condition, Appl. Catal. B Environ. 299 (2021), 120668.

[19] Z. Kou, X. Li, L. Zhang, W. Zang, X. Gao, J. Wang, Dynamic surface chemistry of catalysts in oxygen evolution reaction, Small Sci. 1 (2021), 2100011.

[20] R. Li, P. Kuang, L. Wang, H. Tang, J. Yu, Engineering 2D NiO/Ni_3S_2 heterointerface electrocatalyst for highly efficient hydrogen production coupled with benzyl alcohol oxidation, Chem. Eng. J. 431 (2022), 134137.

[21] S. Wang, Ultrathin carbon encapsulating transition metal-doped MoP electrocatalysts for hydrogen evolution reaction, Acta Phys. Chim. Sin. 37 (2021), 2011013.

[22] L. Fan, T. Meng, M. Yan, D. Wang, Y. Chen, Z. Xing, E. Wang, X. Yang, Rational construction of ruthenium-cobalt oxides heterostructure in ZIFs-derived double-shelled hollow polyhedrons for efficient hydrogen evolution reaction, Small 17 (2021), 2100998.

[23] J. Wang, W. Cui, Q. Liu, Z. Xing, A.M. Asiri, X. Sun, Recent progress in cobalt-based heterogeneous catalysts for electrochemical water splitting, Adv. Mater. 28 (2016) 215–230.

[24] Y. Ha, L. Shi, Z. Chen, R. Wu, Phase-transited lysozyme-driven formation of self-supported Co_3O_4@C nanomeshes for overall water splitting, Adv. Sci. 6 (2019), 1900272.

[25] X. Yan, L. Tian, M. He, X. Chen, Three-dimensional crystalline/amorphous Co/Co_3O_4 core/shell nanosheets as efficient electrocatalysts for the hydrogen evolution reaction, Nano Lett. 15 (2015) 6015–6021.

[26] Z. Xiao, Y. Wang, Y.-C. Huang, Z. Wei, C.-L. Dong, J. Ma, S. Shen, Y. Li, S. Wang, Filling the oxygen vacancies in Co_3O_4 with phosphorus: an ultra-efficient electrocatalyst for overall water splitting, Energy Environ. Sci. 10 (2017) 2563–2569.

[27] H. Jin, J. Wang, D. Su, Z. Wei, Z. Pang, Y. Wang, In situ cobalt-cobalt oxide/N-doped carbon hybrids as superior bifunctional electrocatalysts for hydrogen and oxygen evolution, J. Am. Chem. Soc. 137 (2015) 2688–2694.

[28] K.L. Zhou, C. Wang, Z. Wang, C.B. Han, Q. Zhang, X. Ke, J. Liu, H. Wang, Seamlessly conductive $Co(OH)_2$ tailored atomically dispersed Pt electrocatalyst with a hierarchical nanostructure for an efficient hydrogen evolution reaction, Energy Environ. Sci. 13 (2020) 3082–3092.

[29] Y. Feng, Z. Li, C.-Q. Cheng, W.-J. Kang, J. Mao, G.-R. Shen, J. Yang, C.-K. Dong, H. Liu, X.-W. Du, Strawberry-like Co_3O_4-Ag bifunctional catalyst for overall water splitting, Appl. Catal. B Environ. 299 (2021), 120658.

[30] Z. Fan, J. Jiang, L. Ai, Z. Shao, S. Liu, Rational design of ruthenium and cobalt-based composites with rich metal-insulator interfaces for efficient and stable overall water splitting in acidic electrolyte, ACS Appl. Mater. Interfaces 11 (2019) 47894–47903.

[31] D. Strmcnik, P.P. Lopes, B. Genorio, V.R. Stamenkovic, N.M. Markovic, Design principles for hydrogen evolution reaction catalyst materials, Nano Energy 29 (2016) 29–36.

[32] Z. Wang, W. Xu, X. Chen, Y. Peng, Y. Song, C. Lv, H. Liu, J. Sun, D. Yuan, X. Li, X. Guo, D. Yang, L. Zhang, Defect-rich nitrogen doped Co_3O_4/C porous nanocubes enable high-efficiency bifunctional oxygen electrocatalysis, Adv. Funct. Mater. 29 (2019), 1902875.

[33] J.Y. Zhang, H. Wang, Y. Tian, Y. Yan, Q. Xue, T. He, H. Liu, C. Wang, Y. Chen, B. Y. Xia, Anodic hydrazine oxidation assists energy-efficient hydrogen evolution over a bifunctional cobalt perselenide nanosheet electrode, Angew. Chem. Int. Ed. 57 (2018) 7649–7653.

[34] C. Meng, T. Ling, T.Y. Ma, H. Wang, Z. Hu, Y. Zhou, J. Mao, X.W. Du, M. Jaroniec, S.Z. Qiao, Atomically and electronically coupled Pt and CoO hybrid nanocatalysts for enhanced electrocatalytic performance, Adv. Mater. 29 (2017), 1604607.

[35] S. Zhao, B. Rasimick, W. Mustain, H. Xu, Highly durable and active Co_3O_4 nanocrystals supported on carbon nanotubes as bifunctional electrocatalysts in alkaline media, Appl. Catal. B Environ. 203 (2017) 138–145.

[36] J. Huang, H. Sheng, R.D. Ross, J. Han, X. Wang, B. Song, S. Jin, Modifying redox properties and local bonding of Co_3O_4 by CeO_2 enhances oxygen evolution catalysis in acid, Nat. Commun. 12 (2021) 3036.

[37] J. Xu, C. Zhang, H. Liu, J. Sun, R. Xie, Y. Qiu, F. Lü, Y. Liu, L. Zhuo, X. Liu, J. Luo, Amorphous MoO_X-Stabilized single platinum atoms with ultrahigh mass activity for acidic hydrogen evolution, Nano Energy 70 (2020), 104529.

[38] D. Wang, L. Yang, H. Liu, D. Cao, Polyaniline-coated Ru/$Ni(OH)_2$ nanosheets for hydrogen evolution reaction over a wide pH range, J. Catal. 375 (2019) 249–256.

[39] T. Liu, L. Zhang, B. Cheng, J. Yu, Hollow carbon spheres and their hybrid nanomaterials in electrochemical energy storage, Adv. Energy Mater. 9 (2019), 1803900.

[40] T. Liu, C. Jiang, B. Cheng, W. You, J. Yu, Hierarchical NiS/N-doped carbon composite hollow spheres with excellent supercapacitor performance, J. Mater. Chem. A 5 (2017) 21257–21265.

[41] T. Liu, L. Zhang, W. You, J. Yu, Core-shell nitrogen-doped carbon hollow spheres/Co_3O_4 nanosheets as advanced electrode for high-performance supercapacitor, Small 14 (2018), 1702407.

[42] P. Kuang, Y. Wang, B. Zhu, F. Xia, C.W. Tung, J. Wu, H.M. Chen, J. Yu, Pt single atoms supported on N-doped mesoporous hollow carbon spheres with enhanced electrocatalytic H_2-evolution activity, Adv. Mater. 33 (2021), 2008599.

[43] J. Wang, S. Kaskel, KOH activation of carbon-based materials for energy storage, J. Mater. Chem. 22 (2012) 23710–23725.

[44] P. Wang, H. Ye, Y.X. Yin, H. Chen, Y.B. Bian, Z.R. Wang, F.F. Cao, Y.G. Guo, Fungi-enabled synthesis of ultrahigh-surface-area porous carbon, Adv. Mater. 31 (2019), 1805134.

[45] F. Xu, Z. Tang, S. Huang, L. Chen, Y. Liang, W. Mai, H. Zhong, R. Fu, D. Wu, Facile synthesis of ultrahigh-surface-area hollow carbon nanospheres for enhanced adsorption and energy storage, Nat. Commun. 6 (2015) 7221.

[46] Z. Xing, C. Han, D. Wang, Q. Li, X. Yang, Ultrafine Pt nanoparticle-decorated Co$(OH)_2$ nanosheet arrays with enhanced catalytic activity toward hydrogen evolution, ACS Catal. 7 (2017) 7131–7135.

[47] M. Bajdich, M. Garcia-Mota, A. Vojvodic, J.K. Norskov, A.T. Bell, Theoretical investigation of the activity of cobalt oxides for the electrochemical oxidation of water, J. Am. Chem. Soc. 135 (2013) 13521–13530.

[48] X. Zhao, X. Li, D. Xiao, M. Gong, L. An, P. Gao, J. Yang, D. Wang, Isolated Pd atom anchoring endows cobalt diselenides with regulated water-reduction kinetics for alkaline hydrogen evolution, Appl. Catal. B Environ. 295 (2021), 120280.

[49] X. Cheng, Y. Lu, L. Zheng, Y. Cui, M. Niibe, T. Tokushima, H. Li, Y. Zhang, G. Chen, S. Sun, J. Zhang, Charge redistribution within platinum-nitrogen coordination structure to boost hydrogen evolution, Nano Energy 73 (2020), 104739.

[50] D. Chen, R. Lu, Z. Pu, J. Zhu, H.-W. Li, F. Liu, S. Hu, X. Luo, J. Wu, Y. Zhao, S. Mu, Ru-doped 3D flower-like bimetallic phosphide with a climbing effect on overall water splitting, Appl. Catal. B Environ. 279 (2020), 119396.

[51] J. Xu, T. Liu, J. Li, B. Li, Y. Liu, B. Zhang, D. Xiong, I. Amorim, W. Li, L. Liu, Boosting the hydrogen evolution performance of ruthenium clusters through synergistic coupling with cobalt phosphide, Energy Environ. Sci. 11 (2018) 1819–1827.

[52] K. Jiang, B. Liu, M. Luo, S. Ning, M. Peng, Y. Zhao, Y.R. Lu, T.S. Chan, F.M.F. de Groot, Y. Tan, Single platinum atoms embedded in nanoporous cobalt selenide as electrocatalyst for accelerating hydrogen evolution reaction, Nat. Commun. 10 (2019) 1743.

[53] S. Wang, Y. Cao, W. Jia, Z. Lu, D. Jia, A cage-confinement strategy to fabricate Pt-Mo_6Co_6C heterojunction for highly efficient PH-universal hydrogen evolution, Appl. Catal. B Environ. 298 (2021), 120579.

[54] R. Li, B. Hu, T. Yu, H. Chen, Y. Wang, S. Song, Insights into correlation among surface-structure-activity of cobalt-derived pre-catalyst for oxygen evolution reaction, Adv. Sci. 7 (2020), 1902830.

[55] Z. Chen, Y. Ha, H. Jia, X. Yan, M. Chen, M. Liu, R. Wu, Oriented transformation of Co–LDH into 2D/3D ZIF–67 to achieve Co–N–C hybrids for efficient overall water splitting, Adv. Energy Mater. 9 (2019), 1803918.

[56] B. He, C. Bie, X. Fei, B. Cheng, J. Yu, W. Ho, A.A. Al-Ghamdi, S. Wageh, Enhancement in the photocatalytic H_2 production activity of CdS NRs by Ag_2S and NiS dual cocatalysts, Appl. Catal. B Environ. 288 (2021), 119994.

[57] J. Fu, C. Bie, B. Cheng, C. Jiang, J. Yu, Hollow CoS_x polyhedrons act as high-efficiency cocatalyst for enhancing the photocatalytic hydrogen generation of g-C_3N_4, ACS Sustain. Chem. Eng. 6 (2018), 2767−277.

[58] R. Ge, J. Huo, T. Liao, Y. Liu, M. Zhu, Y. Li, J. Zhang, W. Li, Hierarchical molybdenum phosphide coupled with carbon as a whole pH-range electrocatalyst for hydrogen evolution reaction, Appl. Catal. B Environ. 260 (2020), 118196.

[59] W. Zhao, C. Luo, Y. Lin, G. Wang, H.M. Chen, P. Kuang, J. Yu, Pt−Ru dimer electrocatalyst with electron redistribution for hydrogen evolution reaction, ACS Catal. 12 (2022) 5540–5548.

[60] K.L. Zhou, Z. Wang, C.B. Han, X. Ke, C. Wang, Y. Jin, Q. Zhang, J. Liu, H. Wang, Hui Yan, Platinum single-atom catalyst coupled with transition metal/metal oxide heterostructure for accelerating alkaline hydrogen evolution reaction, Nat. Commun. 12 (2021) 3783.